The Crystal Structure of the Ternary Complex of Phenylalanyl-tRNA Synthetase with $tRNA^{Phe}$ and a Phenylalanyl-Adenylate Analogue Reveals a Conformational Switch of the CCA End†

Nina Moor,‡,§ Olga Kotik-Kogan,§,|| Dmitry Tworowski,|| Maria Sukhanova,‡ and Mark Safro*,||

Department of Structural Biology, Weizmann Institute of Science, 76100 Rehovot, Israel, and Institute of Chemical Biology and Fundamental Medicine, 630090 Novosibirsk, Russia

Received March 12, 2006; Revised Manuscript Received July 12, 2006

ABSTRACT: The crystal structure of the ternary complex of $(\alpha\beta)_2$ heterotetrameric phenylalanyl-tRNA synthetase (PheRS) from *Thermus thermophilus* with cognate $tRNA^{Phe}$ and a nonhydrolyzable phenylalanyl-adenylate analogue (PheOH-AMP) has been determined at 3.1 Å resolution. It reveals conformational changes in $tRNA^{Phe}$ induced by the PheOH-AMP binding. The single-stranded 3′ end exhibits a hairpin conformation in contrast to the partial unwinding observed previously in the binary PheRS·$tRNA^{Phe}$ complex. The CCA end orientation is stabilized by extensive base-specific interactions of A76 and C75 with the protein and by intra-RNA interactions of A73 with adjacent nucleotides. The 4-amino group of the "bulged out" C75 is trapped by two negatively charged residues of the β subunit (Gluβ31 and Aspβ33), highly conserved in eubacterial PheRSs. The position of the A76 base is stabilized by interactions with Hisα212 of motif 2 (universally conserved in PheRSs) and class II-invariant Argα321 of motif 3. Important conformational changes induced by the binding of $tRNA^{Phe}$ and PheOH-AMP are observed in the catalytic domain: the motif 2 loop and a "helical" loop (residues 139−152 of the α subunit) undergo coordinated displacement; Metα148 of the helical loop adopts a conformation preventing the 2′-OH group of A76 from approaching the α-carbonyl carbon of PheOH-AMP. The unfavorable position of the terminal ribose stems from the absence of the α-carbonyl oxygen in the analogue. Our data suggest that the idiosyncratic feature of PheRS, which aminoacylates the 2′-OH group of the terminal ribose, is dictated by the system-specific topology of the CCA end-binding site.

Aminoacyl-tRNA synthetases (aaRSs)[1] promote close control over two-step aminoacylation reaction, establishing a linkage between cognate amino acid and three nucleotides of the tRNA anticodon(s). In the first step, an aminoacyl-adenylate is synthesized from the amino acid and ATP. In the second step, the activated amino acid is transferred to the 3′ end of the cognate tRNA. Comprehensive analysis of aaRS sequences and three-dimensional (3D) structures led to discovery of common structural features and, further, to the partitioning of the aaRS family into two classes (*1*, *2*). The classification remarkably correlates with two modes of attack on the aminoacyl-adenylate carbonyl: the 2′-OH group of the tRNA 3′-terminal ribose is the primary site of aminoacylation for class I and the 3′-OH group for class II. Phenylalanyl-tRNA synthetase (PheRS) is the only exception to this rule: being the class II enzyme in accordance with structural classification, it attaches phenylalanine to the 3′-terminal 2′-OH of $tRNA^{Phe}$ (*3*, *4*). The chemical mechanism of the aminoacylation reaction is essentially conserved in both classes (*5*); however, each synthetase is unique in the modes of recognition of the amino acid and tRNA substrates (reviewed in refs *5*−*8*).

The structure of aspartyl-tRNA synthetase (AspRS) is one of the best-documented class II structures. Reported for evolutionarily diverged species, AspRS complexes with various combinations of substrates (refs *9*−*13* and references cited therein) provide snapshots of the aspartylation reaction. The binding of aspartic acid gives rise to conformational changes in the class II-conserved motif 2 loop and a so-called "flipping" loop, which secure the position of the aminoacyl moiety for adenylate synthesis. Formation of the catalytically competent AspRS·$tRNA^{Asp}$ complex is accompanied by conformational changes in both macromolecules to optimize the mutual fit. The $tRNA^{Asp}$ acceptor arm and the AMP moiety are positioned by the motif 2 loop; in the absence of ATP, the 3′-terminal adenosine (A76)

† This work was supported by Kimmelman Center for Biomolecular Structure and Assemblies and by a grant to M. Safro from the Israel Science Foundation (1034/03). N.M. was supported in part by the Russian Foundation for Basic Research (Grants 03-04-48384 and 06-04-48798) and by the Siberian Branch of the Russian Academy of Sciences (grant 110). M. Safro holds the Lee & William Abramowitz Professorial Chair of Molecular Biophysics.

* To whom correspondence should be addressed. E-mail: mark.safro@weizmann.ac.il. Fax: 972-8-934-41-36. Phone: 972-8-934-33-20.

‡ Institute of Chemical Biology and Fundamental Medicine.

§ These authors contributed equally to this work.

|| Weizmann Institute of Science.

[1] Abbreviations: aaRS(s), aminoacyl-tRNA synthetase(s); PheRS, phenylalanyl-tRNA synthetase; AspRS, aspartyl-tRNA synthetase; SerRS, seryl-tRNA synthetase; ThrRS, threonyl-tRNA synthetase; ArgRS, arginyl-tRNA synthetase; GlnRS, glutaminyl-tRNA synthetase; GluRS, glutamyl-tRNA synthetase; PheOH-AMP, L-phenylalaninyl-5′-adenylate; Phe-AMP, L-phenylalanyl-5′-adenylate; MD, molecular dynamics; s^4U, 4-thiouridine; s^6G, 6-thioguanosine.

10.1021/bi060491l CCC: $33.50
Published on Web 08/15/2006

occupies the ATP binding site (*9*). Switching to the open conformation is necessary for the flipping loop to anchor the base of A76 and place it in the proper position within the active site. The interrelation between the binding of the tRNA 3′ end and that of small substrates has been shown for other aaRSs. Binding of the $tRNA^{Ser}$ acceptor arm to seryl-tRNA synthetase (SerRS) depends critically on the positioning of the motif 2 loop, which is disordered in the absence of any substrates and adopts two different conformations in the presence of $tRNA^{Ser}$ and ATP or adenylate (*14*). A number of residues that interact with a seryl-adenylate analogue (Ser-AMS) switch to participate in the $tRNA^{Ser}$ recognition when viewed for the ternary SerRS·$tRNA^{Ser}$·Ser-AMS complex. Four mobile regions of the catalytic domain of threonyl-tRNA synthetase (ThrRS) are involved in correct positioning of the $tRNA^{Thr}$ acceptor arm; residues initially implicated in threonine or ATP binding switch to the recognition of the tRNA 3′ end (*15*). In addition, transformations of flexible regions upon binding of the small substrates have been reported for several class II systems (*16*−*19*). Notably, three of the class I aaRSs, arginyl-, glutaminyl-, and glutamyl-tRNA synthetases (ArgRS, GlnRS, and GluRS, respectively), which catalyze amino acid activation only in the presence of their cognate tRNAs, exhibit different relationships between the substrates. While the 3′-terminal nucleotide of $tRNA^{Gln}$ forms part of the glutamine-binding site (*20*), the correct positioning of the $tRNA^{Arg}$ CCA end is controlled by the arginine binding (*21*). The binding of $tRNA^{Glu}$ to GluRS triggers structural changes required for productive interaction with ATP, and this regulation mechanism seems to be universal for the tRNA-dependent triad (*22*). Examples of the great diversity of available data show that the peculiarity of the aminoacylation site in each amino acid system is governed by stepwise fine adjustment of all the reactants and their intermediates.

PheRS is one of the most complex enzymes of the aaRS family; the tetrameric $(\alpha\beta)_2$ subunit organization of cytoplasmic PheRS is markedly conserved through evolution. Several 3D structures of *Thermus thermophilus* PheRS, both native and in complexes with substrates, are available (*23*−*27*). PheRS is a functional dimer (reviewed in ref *28*). The $\alpha\beta$ heterodimer consists of 11 structural domains: three of them (a coiled-coil arm at the N-terminus, A1, and A2) belong to the α subunit and eight (B1−B8) to the large β subunit. Domains A1 and A2 create the class II-conserved catalytic module; the major function of the β subunit is in binding and recognition of $tRNA^{Phe}$. The modes of $tRNA^{Phe}$ recognition by PheRSs of evolutionarily diverged species have been analyzed by in vitro aminoacylation of $tRNA^{Phe}$ mutants (reviewed in ref *28*). The anticodon nucleotides are the major determinants of $tRNA^{Phe}$ specificity in all systems. The contribution of nucleotides 20 and 73 and of A31·U39 and G30·C40 base pairs to the aminoacylation efficiency varies greatly; it was found to be minor in the *Escherichia coli* and *T. thermophilus* systems. On the basis of independent measurements of binding and aminoacylation of $tRNA^{Phe}$ mutants with *T. thermophilus* PheRS, tertiary nucleotides have been subdivided into two groups according to their major functional role in determining the precise $tRNA^{Phe}$ structure. The G19·C56 base pair and U45·G10·C45 base triple contribute mostly to stabilization of the overall folding; the A26·G44 base pair is involved in the conformational adjustment of the tRNA upon its interaction with the enzyme (*29*). Biochemical studies of the *T. thermophilus* PheRS·$tRNA^{Phe}$ complex (*30*, *31*) are in agreement with the X-ray data, while having revealed dynamic interactions in the structure. The position of A76 in the binary PheRS·$tRNA^{Phe}$ complex (*24*) partially interferes with the location of the phenylalanine substrate in the active site (*25*, *26*). The affinity−cross-linking data obtained for *T. thermophilus* and human PheRSs (*32*−*34*) give an indication of acceptor end rearrangement in the presence of other substrates: the interaction of the enzyme with phenylalanine and ATP and the synthesis of adenylate affect the orientation of the tRNA 3′ end. Evidently, the proper positioning of the $tRNA^{Phe}$ acceptor end corresponding to the structure of the productive complex is promoted only in the presence of a phenylalanyl-adenylate.

Here, we describe the crystal structure of *T. thermophilus* PheRS in a complex with homologous $tRNA^{Phe}$ cocrystallized in the presence of a stable phenylalanyl-adenylate analogue. Molecular dynamics calculations for various binary complexes of the enzyme with functional ligands have also been carried out. Our data combined with previously determined binary PheRS complexes provide multiple snapshots of different stages of the phenylalanylation reaction and enable us to follow the mutual adjustment of the enzyme and substrates in a precise manner. Analysis of the available complexes has yielded structural elements of PheRS that are responsible for the correct positioning of the functional ligands within the active site.

EXPERIMENTAL PROCEDURES

Crystallization. Native PheRS from *T. thermophilus* strain HB8 was isolated and purified as described previously (*35*). *T. thermophilus* $tRNA^{Phe}$ (isoacceptor I, 1700 pmol of Phe/A_{260} unit) was purified using procedures developed by Watanabe et al. (*36*) and Bischoff and McLaughlin (*37*). L-Phenylalaninyl-5′-adenylate (PheOH-AMP) was synthesized and purified as described previously (*38*). Crystals of the PheRS·$tRNA^{Phe}$·PheOH-AMP complex were grown at 4 °C by the hanging-drop vapor-diffusion method. The solution for cocrystallization was prepared at a final protein concentration of 3−5 mg/mL for molar ratios of PheRS and $tRNA^{Phe}$ of 1:2.5 in a buffer [20 mM imidazole-HCl (pH 7.8), 1 mM $MgCl_2$, 5 mM 2-mercaptoethanol, and 1 mM NaN_3] containing 10% saturated ammonium sulfate and 1 mM PheOH-AMP. The drop solution was slowly equilibrated against a reservoir solution containing the crystallization buffer and 27% saturated ammonium sulfate. The crystals of the ternary complex belong to the same space group, $P3_221$, and have virtually the same unit cell parameters as crystals of native PheRS and the binary PheRS·$tRNA^{Phe}$ complex (*39*).

Data Collection. Diffraction data were collected on beamline ID14 at the synchrotron radiation source at ESRF (Grenoble, France) and with in-house Rigaku R-axis IV^{++} image plate detector. Before being flash-cooled, the crystals of the PheRS·$tRNA^{Phe}$·PheOH-AMP complex were transferred into a cryoprotectant containing the reservoir solution and 30% (v/v) glycerol. Diffracted intensities were evaluated and integrated using the HKL package (*40*) and scaled further using programs from the CCP4 package.

Table 1: Data Collection and Refinement Statistics for the PheRS·tRNA^{Phe}·PheOH-AMP Complex

	native PheRS (1PYS)	PheRS·tRNA^{Phe}·PheOH-AMP
diffraction data		
space group	$P3_221$	$P3_221$
unit cell parameters (Å)	$a = b = 176.3$, $c = 141.0$	$a = b = 173.4$, $c = 139.4$
resolution (Å)	2.9	3.1
total no. of reflections	307528	273326
no. of unique reflections	59314	39855
completeness (%)	97.6	89.0
R_{merge}[a] (%)	7.2	11.2
refinement statistics		
resolution range (Å)	50−2.9	50−3.1
no. of protein atoms	8250	8765
no. of tRNA atoms		1618
no. of PheOH-AMP atoms		31
no. of water molecules	331	185
R_{work}/R_{free}[b] (%)	17.7/23.6	22.36/29.50
rms deviation		
bond lengths (Å)	0.011	0.008
bond angles (deg)	1.72	1.43

[a] $R_{merge} = \sum_{hkl}|I_j(hkl) - \langle I_j(hkl)\rangle|/\sum_{hkl}\sum I_j(hkl)$, where $I_j(hkl)$ and $\langle I_j(hkl)\rangle$ are the intensity of measurement j and the mean intensity for the reflection with indices hkl, respectively. [b] R factor $= \sum(F_{obs} - kF_{calc})/\sum_{hkl}F_{obs}$, where k is a scale factor and R_{free} is the R factor for the test set of reflections. The data for the native PheRS structure (1PYS) are from ref *23*.

Structure Determination and Refinement. The 2.9 Å refined model of *T. thermophilus* PheRS (*23*) was used as a starting model. This model was first subjected to rigid-body refinement using a 50−3.1 Å resolution data set of the PheRS·tRNA^{Phe}·PheOH-AMP complex. The initial R factor of 50.1% was reduced to 37.2% by rigid-body refinement. The subsequent refinement procedures (conjugate-gradient energy minimization, combined simulated annealing, and B factor refinement) were carried out using CNS (*41*). In accordance with the difference electron density maps, 70 amino acids from the N-terminus of the α subunit were added manually to the starting model, and the whole molecule was subjected to several rounds of conjugate-gradient minimization. However, electron density associated with the first 15 residues of the α subunit remains relatively poor; these residues were not included in the final model.

The model of tRNA was built into the density with O (*42*). Refinement of the complex was carried out by using conjugate-gradient minimization and simulated annealing protocols. With simulated annealing procedures, the temperature factors were fixed to the value of 80 Å^2; the molecular dictionary file maintained the restraints of the DNA−RNA conformation. The data collection and refinement statistics are summarized in Table 1.

Molecular Dynamics Simulations. Molecular dynamics (MD) simulations were carried out using GROMACS version 3.21 (http://www.gromacs.org) (*43*, *44*) with the GROMOS-96 43A2 force field (*44*, *45*). The bonding parameters for phenylalanyl-adenylate (Phe-AMP) and PheOH-AMP were taken from the standard GROMOS96 force field provided by the PRODRG2.5 server (beta version, http://davapc1.bioch.dundee.ac.uk/cgi-bin/prodrg_beta). For these ligands, the GROMACS topology files were generated by using PRODRG (*46*). The 3D structure of Phe-AMP is based on the conformation that adopts PheOH-AMP in the ternary PheRS·tRNA^{Phe}·PheOH-AMP complex. The starting coordinates for the PheRS·PheOH-AMP complex were taken from the ternary complex. Polar and aromatic hydrogen atoms were added to the protein and the ligand atoms. Protonated states of the residues that corresponded to pH 7 were chosen. The protein was then centered in a rectangular box with dimensions such that the distance between the protein and the walls of the box was more than 0.6 nm in each direction. The dimensions of the box were 11.7 nm × 6.81 nm × 7.18 nm. The box was filled with water molecules modeled as single-point charges. The water configuration was relaxed using 50 cycles of energy minimization while keeping the protein frozen. Then, all degrees of freedom of the system were relaxed with another 50 cycles of energy minimization.

The conditions of a constant number of particles, constant pressure, and constant temperature (NPT) were used in simulation. A production simulation of 3 ns was run for the whole system after equilibration for 1000 ps. The time step was 2 fs, with constrained bond lengths; trajectory data were collected every 50 steps (0.1 ps). A constant pressure (p = 101 325 Pa) and a constant temperature (T = 300 K) were used, by weakly coupling the protein and solvent separately to an external bath (t_T = 0.1 ps and t_p = 1.0 ps). A twin-range cutoff method was used for nonbonded interactions. Lennard-Jones and Coulomb interactions within 0.8 nm were recalculated every time step, whereas nonbonding interactions between 0.8 and 1.4 nm were updated every five steps.

RESULTS

Overview of the PheRS·tRNA^{Phe}·PheOH-AMP Complex. The crystal structure of the ternary complex of *T. thermophilus* PheRS with homologous tRNA^{Phe} and a nonhydrolyzable phenylalanyl-adenylate analogue, PheOH-AMP, has been determined at 3.1 Å resolution (Figure 1). The unbiased difference map with amplitudes and phases based on the model of the native protein (*23*) exhibited a well-defined density for the aminoacyl-adenylate analogue at the active site (Figure 2A) and a density for the most of the tRNA molecule. Characteristic density for two long antiparallel α helices appeared immediately after Argα85. Several rounds of conjugate-gradient energy minimization and simulated annealing, alternating with manual revision using O (*42*), resulted in construction of the entire tRNA^{Phe} molecule.

The ternary complex structure presented here is consistent with previously determined structures of the binary PheRS complexes with tRNA^{Phe}, Phe-AMP, or PheOH-AMP (*24*−*26*). Each of the two tRNAs interacts with all four subunits of the heterotetramer. While the acceptor stem and the CCA end of tRNA^{Phe} are localized in the area of the active site of the α subunit and contact domains B1, B3, and B7 from the same αβ heterodimer, the anticodon arm and the variable loop are clamped between the B8 domain and the N-terminal helical arm of the α subunit from the symmetry-related heterodimer (Figure 1). Substantial conformational changes of the protein induced by the tRNA are evidenced by ordering of N-terminal residues in the α subunit. It must be emphasized that in the structure of native PheRS as well as in the complexes with small substrates (Phe, Phe-AMP, Tyr, etc.) the first 84 residues of the N-terminus in the α subunit are disordered. The stabilization of the helical arm, revealed in

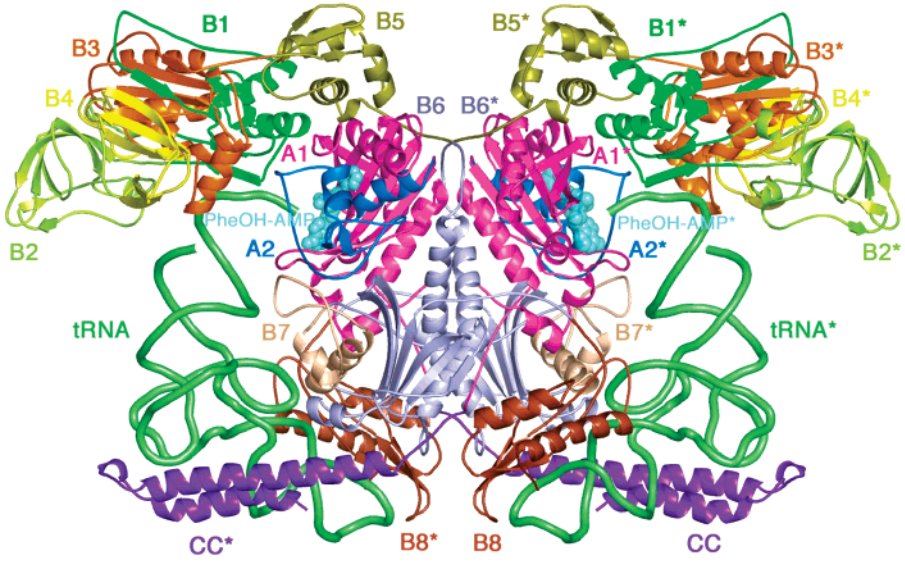

FIGURE 1: Structure of the dimeric *T. thermophilus* PheRS·tRNA^{Phe}·PheOH-AMP complex. The protein and tRNA (mint green) are shown in worm representation; the ligand (PheOH-AMP) is shown in space-filling representation (cyan). The domain architecture of one $\alpha\beta$ heterodimer is shown with the N-terminal coiled coil of the α subunit (residues 1−101) colored purple, catalytic domains A1 (residues 102−125 and 192−350) and A2 (residues 126−191) colored magenta and blue, respectively, β subunit domain B1 (residues 1−39 and 152−183) colored bright green, B2 (residues 40−151) colored lime, B3 (residues 211−264 and 329−396) colored gold, B4 (residues 265−328) colored yellow, B5 (residues 401−473) colored olive, B6 (residues 482−514 and 564−679) colored powder blue, B7 (residues 515−563) colored light brown, and anticodon-binding domain B8 (residues 692−785) colored brown. The structural domains associated with the symmetry-related heterodimer (colored with the same colors) are denoted with asterisks. The ternary complex is PDB entry 2iy5.

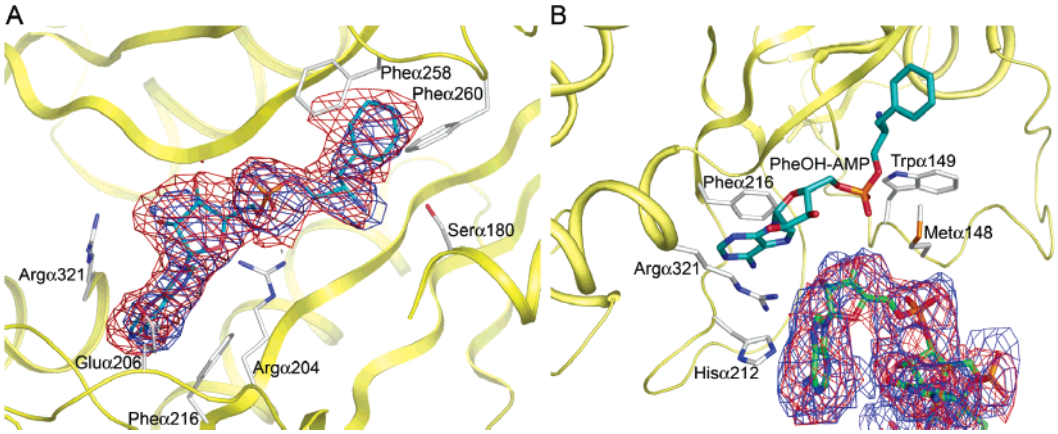

FIGURE 2: Positions of the tRNA^{Phe} CCA end and PheOH-AMP in the active site of PheRS. (A) Part of the electron density map in the close vicinity of PheOH-AMP, calculated with coefficients $F_{obs} - F_{calc}$ (unbiased, colored blue, 1PYS) and $2F_{obs} - F_{calc}$ (refined model, colored red) contoured at 3.5σ and 1.0σ, respectively. (B) Part of the electron density map in the close vicinity of the tRNA^{Phe} 3′ end, calculated with coefficients $F_{obs} - F_{calc}$ (unbiased, colored blue, 1PYS) and $2F_{obs} - F_{calc}$ (refined, colored red) contoured at 2.0σ and 1.0σ, respectively. The CCA end (represented as a stick model colored mint green, blue, and red) is bent in the presence of PheOH-AMP.

the ternary complex and previously in the binary PheRS·tRNA^{Phe} complex (*24*), can be explained on the basis of its intensive contacts with the tRNA. However, the electron density corresponding to the first 15 residues at the N-terminus remains relatively poor, and they have not been included in the final model. Few C-terminal residues of the β subunit (781−785) are also not visible in the electron density map.

Comparison of the Overall Modes of tRNA^{Phe} Binding and Recognition in the PheRS·tRNA^{Phe}·PheOH-AMP and PheRS·tRNA^{Phe} Complexes. In the ternary complex structure presented here, the binding mode of the anticodon arm contributing mostly to the tRNA^{Phe} recognition (reviewed in ref *28*) is largely similar to that revealed in the previous structure of the binary PheRS·tRNA^{Phe} complex (*24*). G34, the major identity element of tRNA^{Phe} in the *T. thermophilus* system (*29*, *47*), makes base-specific interactions with Serβ*742 and Aspβ*729 as well as a stacking with Tyrβ*731 (residues from the symmetry-related heterodimer are marked with an asterisk). Minor conformational changes produce one more specific hydrogen bond between the guanidinium group of Argβ*780 and the O6 atom of G34. This interaction is supplementary to the hydrogen bond between Argβ*780 and the N7 atom of G34 observed in the binary complex structure (*24*). Thus, the synthetase recognition of G34 in the PheRS·tRNA^{Phe}·PheOH-AMP ternary complex is enhanced by the fourth base-specific hydrogen bond with Argβ*780. All the residues mentioned above belong to domain B8 from the symmetry-related heterodimer and are highly conserved or invariant in eubacterial PheRSs. Both A35 and A36 in the ternary complex retain interactions characteristic of the binary PheRS·tRNA^{Phe} complex (*24*). The anticodon loop confor-

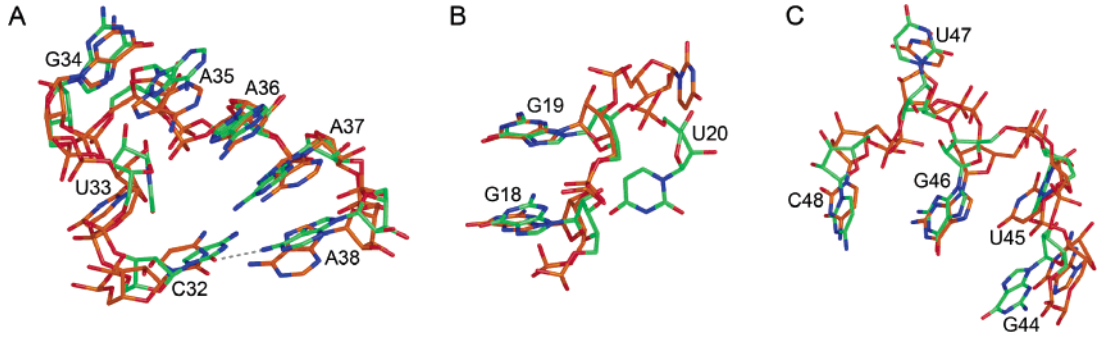

FIGURE 3: Comparison of the tRNA^{Phe} structures in binary PheRS·tRNA^{Phe} and ternary PheRS·tRNA^{Phe}·PheOH-AMP complexes. Structural alignment of the tRNA^{Phe} anticodon loop (A), the D loop fragment of residues 18−20 (B), and the variable loop (C) observed in the ternary (colored mint green, blue, and red) or binary complexes (colored light brown, blue, and red; PDB entry 1EIY). The hydrogen bond between C32 and A38 is represented as a dashed line.

mation is stabilized further by intra-RNA interactions not detected previously in the absence of PheOH-AMP (Figure 3A). The base of C33 is displaced in a way that favors hydrogen bonding between its N3 atom and the O1P atom of A36, as observed in the recently revisited structure of free yeast tRNA^{Phe} (*48*, *49*). A new hydrogen bond is formed between O2 of C32 and N6 of A38. The C32·A38 pair was shown to participate in stabilization of the anticodon arm and strengthening of the base pair between residues 31 and 39 in tRNA^{Lys} (*50*). Several examples of tRNA−aaRS complexes with at least one hydrogen bond between bases 32 and 38 (*22*, *51*) and formation of the U32·A38 Watson−Crick pair in the case of tRNA$^{Pro(CGG)}$ (*52*) are evidence of this interaction being important for supporting the anticodon hairpin conformation (for a review, see ref *53*).

Additional conformational changes are observed in single-stranded regions away from the catalytic site. In the D loop, nucleotides 16 and 17 are rearranged to the "bulged-out" orientation that leads to disruption of the tertiary H-bond interaction between U16 and U59 shown previously to occur in the binary PheRS·tRNA^{Phe} complex. The position of G18 dictated by the displacement of the two former nucleotides allows its tertiary interaction with ψ55 observed previously in the binary complex. The G19·C56 Watson−Crick pair is also conserved in the ternary complex to stabilize the intramolecular interaction between the T and D loops. The D20 base is directed toward the interior of the D loop in our complex, while it is splayed out in the binary complex (Figure 3B). Of these nucleotides, only G19 and C56 are involved in backbone-mediated interactions of the tRNA^{Phe} core with the N-terminal coiled-coil domain of the α subunit. D16 and D20 contribute to different extents to tRNA^{Phe} recognition (*29*, *47*), while they do not contact the enzyme in any structure. Significant conformational changes of PheRS (as compared to the binary PheRS·tRNA^{Phe} complex) are observed for the segment of residues 30−58 at the end of the helical arm. However, its interactions with G19 and C56 either remain unchanged or are replaced by similar interactions with adjacent residues of the segment (data no shown). The relative position of the coiled-coil domain in the ternary complex is very similar to that found in the binary complex. The domain designed to anchor the tRNA is characterized by a high degree of flexibility (reflected in relatively high atomic temperature factors), which ensures a good adaptability. The variable loop, comprising nucleotides 44−48, is the third region where conformational changes are worthy of notice. This region shown to contribute to tRNA^{Phe} recognition via determination of its precise conformation (*29*, *47*) is also involved in the backbone-mediated contacts with the coiled-coil domain (residues 17−28). Two nucleotides, G44 and U47, adopt new conformations; G44 involved in a stacking interaction with A43 and U45 in the PheRS·tRNA^{Phe} complex is flipped out in the ternary complex (Figure 3C). The rearrangement results in disruption of the noncanonical tertiary interaction of nucleotide 44 with nucleotide 26 formed in both free yeast tRNA^{Phe} (G44·A26) and the *T. thermophilus* PheRS·tRNA^{Phe} complex (A26·G44). The variable loop conformation is therefore stabilized by two tertiary base pairing interactions (of U45 with the G10·C25 Watson−Crick pair through the triple contacts and of C48 with G15) as well as by intermolecular contacts with the N-terminal helical arm.

Acceptor Arm Binding and Recognition. The acceptor arm of tRNA^{Phe} is positioned within a wide cavity formed by structural domains that belong to the common $\alpha\beta$ heterodimer (Figure 1). The CCA extremity makes both base-specific and sugar- and phosphate-mediated contacts with the catalytic A1−A2 module and domains B1 and B3 (Table 2). A limited number of contacts between the protein and the sugar−phosphate backbone of tRNA^{Phe} are found along the acceptor stem; these contacts are nonspecific and water-mediated. Substantial conformational changes are evident when the CCA end is compared with that of the PheRS·tRNA^{Phe} complex (Figure 4). In the ternary complex, the single-stranded region exhibits a hairpin conformation (see also Figure 2B) contrary to the partial unwinding observed in the binary complex. The hairpin structure is reminiscent of those observed in the class I GlnRS, ArgRS, and GluRS complexed with their cognate tRNAs (*20*−*22*) and stabilized by system-specific molecular mechanisms. As a consequence of the rearrangement, the sugar- and phosphate-mediated contacts of the ACCA end with domain B1 are lost (Table 2). Two residues from domain B3, Hisβ358 and Argβ362, which anchor the ribose moiety of C74 in the absence of PheOH-AMP, now interact with the phosphate group of C75. Another positively charged residue from domain B3, Argβ353, forms a contact with the phosphate group of C74, thus reinforcing the cluster of nonspecific interactions. This residue is conserved in half the known sequences of eubacterial PheRSs and replaced in some species with His or Lys. The CCA end orientation is stabilized further by extensive base-specific interactions of A76 (described below) and C75. The 4-amino group of the bulged-out C75 is trapped by the negatively charged side chains of Gluβ31 and Aspβ33,

Table 2: Comparison of Interactions of the $tRNA^{Phe}$ Acceptor End with PheRS in the Binary and Ternary Complexes[a]

	PheRS·$tRNA^{Phe}$			PheRS·$tRNA^{Phe}$·PheOH-AMP		
tRNA	protein residue (domain/motif)	distance (Å)	type	protein residue (domain/motif)	distance (Å)	type
A76 base	**Phe**α258[b] ring (A1)	4.6	AA	**His**α212 ring (motif 2)	3.4	AA, π−cation
A76 base	**Phe**α260[b] ring (A1)	5.2	AA	AMP*	5.3	AA
A76 N7	Trpα149 Nε1 (A2)	2.9	HB	***Arg***α321 Nη1, Nη2 (motif 3)	3.3, 3.1	HB
A76 N6	**Ser**α180 Oγ (A2)	3.6	HB			
A76 N6	**Glu**α220 Oε1 (A1)	3.0	HB			
A76 O3′				***Arg***α204 Nη1 (motif 2)	2.7	HB
A76 O3′				**Met**α148[c] O (A1)	3.5	HB
A76 O3′				**Met**α148[c] Sδ (A1) (via water 67)	3.0 and 3.1	HB
A76 O2′				**Glu**α206 Oε1 (motif 2)	3.1	HB
C75 N4				**Glu**β31 Oε2 (B1)	3.1	HB
C75 N4				**Asp**β33 Oδ1 (B1)	2.7	
C75 O1P	**Val**β160 N (B1)	3.4	HB	Hisβ358 Nδ1 (B3)	4.2	ES
C75 O2P				**Arg**β362 Nη2 (B3)	3.1	HB
C74 O2′	Hisβ358 Nε2 (B3)	3.3	HB			
C74 O2′	**Arg**β362 Nη1 (B3)	3.7	HB			
C74 O1P	Argβ2 Nη1 (B1)	3.4	HB			
C74 O2P	**Met**β1 N (B1)	4.5	ES	Argβ353 Nη2 (B3)	2.7	HB
A73 O2P	Argβ2 Nη2 (B1)	3.9	ES/HB			

[a] Indicated tRNA contacts with protein residues and the AMP* moiety of PheOH-AMP are made by hydrogen bonds (HB) and aromatic−aromatic (AA), electrostatic (ES), and π−cation interactions; PheRS domains or class II signature motifs are given in parentheses. For water-mediated interactions, two distances between the donor atom and water and between the water and the acceptor atom are indicated; amino acid residues conserved (invariant or replaced with similar residues) in all PheRSs are in bold type, those specific for eubacteria underlined, and class II invariants in italic type. [b] This residue belongs to the FPF loop (residues 256−264). [c] This residue belongs to the helical loop (residues 139−152).

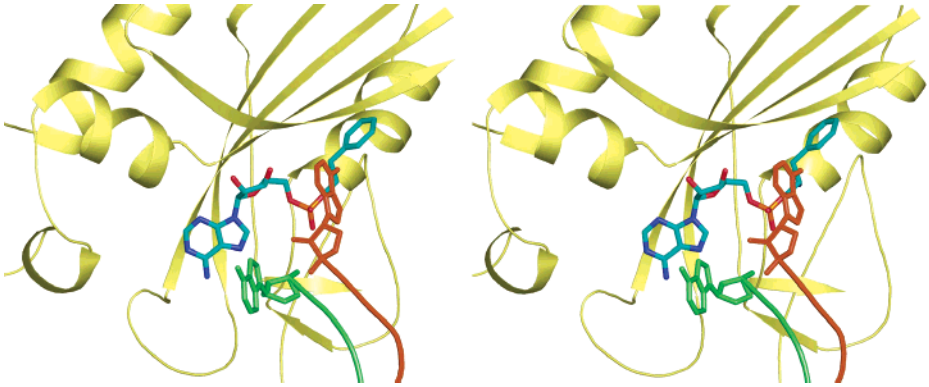

FIGURE 4: Conformational changes of the $tRNA^{Phe}$ acceptor end in the complex with PheRS, induced by the bound PheOH-AMP. The stereoview shows the positioning of A76 in the ternary PheRS·$tRNA^{Phe}$·PheOH-AMP complex (mint green) as compared to that observed in the binary PheRS·$tRNA^{Phe}$ complex (light brown). The terminal nucleotide is rearranged in the presence of PheOH-AMP due to competition with the Phe moiety of the analogue for interactions with the enzyme residues.

highly conserved in eubacterial PheRS acidic residues belonging to domain B1. A73, a minor recognition element of $tRNA^{Phe}$ by *T. thermophilus* PheRS (*29*, *47*), does not participate in interactions with the protein. This nucleotide is stacked on the first base pair of the tRNA and forms a hydrogen bond involving its 6-amino group and O2 of C74, thus contributing to stabilization of the hairpin structure of the CCA end.

Active Site Rearrangement upon $tRNA^{Phe}$ and PheOH-AMP Binding. A continuous and contrasted (>3.5σ) electron density allows a clear characterization of the PheOH-AMP analogue in the active site of the enzyme (Figure 2A). The difference between the phenylalanyl-adenylate analogue and its nonhydrolyzable analogue is in the replacement of the carbonyl group by the CH_2 group. It is of interest that despite the medium resolution the bulge corresponding to the carbonyl oxygen is absent from the electron density. In the ternary complex, the PheOH-AMP analogue occupies the position in the active site closely similar to those observed in the binary PheRS·PheOH-AMP and PheRS·Phe-AMP complexes (*25*, *26*). The rmsd for the adenylate analogue from our complex superimposed on the native intermediate in the PheRS·Phe-AMP complex is 0.9 Å.

The amino acid moiety of the phenylalaninyl-adenylate analogue is stabilized by aromatic−aromatic interactions with eubacterial PheRSs-conserved residues, Pheα258 and Pheα260 (Figure 2A). The α-NH_3^+ group of PheOH-AMP is involved in hydrogen bonding with Serα180, Hisα178, and Gluα220 (Figure 5). A class II-invariant Argα204 of the motif 2 loop adopts an extended conformation in comparison with that in the native structure and interacts with the phosphate group of the PheOH-AMP analogue. The AMP moiety is sandwiched between the side chains of class II-conserved residues, Pheα216 of motif 2 and the hydrophobic part of motif 3 Argα321 (Figure 2). The detailed scheme of interactions of the adenylate analogue within the active site has been presented previously for the binary PheRS·PheOH-AMP complex (*25*); the interactions are retained with no modifications in the presence of $tRNA^{Phe}$.

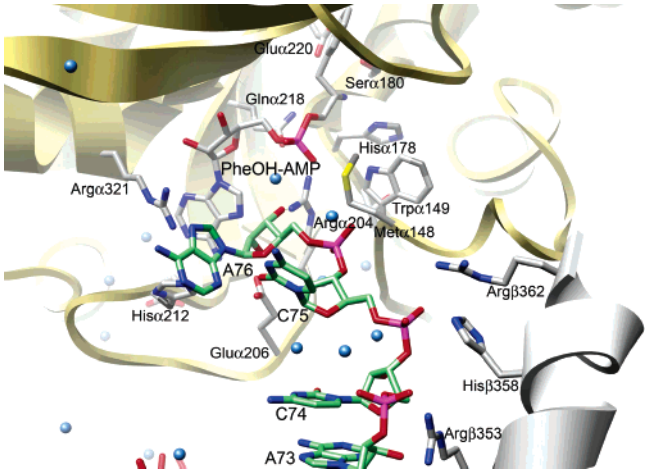

FIGURE 5: Ribbon and stick representation of the active site of *T. thermophilus* PheRS with bound PheOH-AMP and the 3′-ACCA end of $tRNA^{Phe}$. The $tRNA^{Phe}$ 3′ end colored mint green is shown in the foreground. The adenylate analogue is depicted in the background. Water molecules are depicted as blue spheres. The main chain of PheRS is shown as ribbons colored light yellow and gray for the α and *β* subunits, respectively.

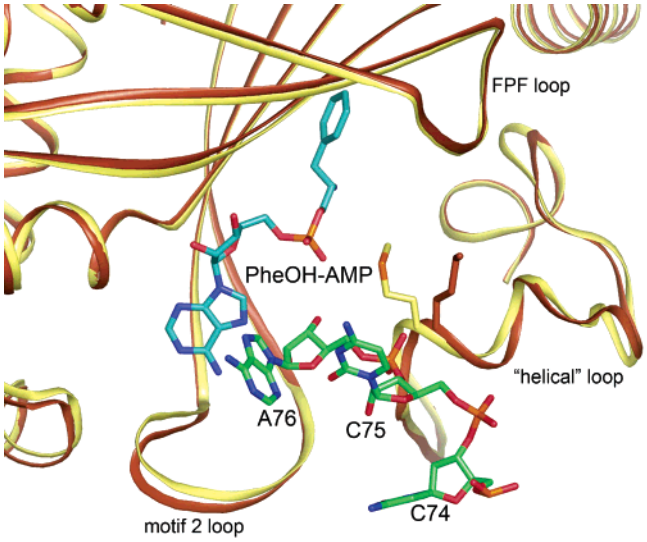

FIGURE 6: Diagram showing conformational changes of helical and motif 2 loops in the ternary complex of PheRS upon substrate binding as compared to the apo form of the enzyme. PheRS (colored light yellow) in the ternary complex with $tRNA^{Phe}$ (mint green) and PheOH-AMP (ice blue) is superimposed with PheRS in the apo form (light brown). The motif 2 (residues 204−214) and helical loops (residues 139−152) move toward the bound ligands, while the conformation of the phenylalanine-binding FPF loop (residues 256−264) is unaffected. The side chain of Metα149 in the helical loop displays the most significant conformational switch in the active site; in fact, this residue controls the opening and closing of the active site cavity and thus the correct order of substrate binding and the reaction.

Superposition of two binary complexes of *T. thermophilus* PheRS with $tRNA^{Phe}$ and the phenylalanyl-adenylate alone, as presented in Figure 4, shows partial interference of the $tRNA^{Phe}$ terminal adenosine (A76) and the amino acid moiety of Phe-AMP (*26*). The acceptor end repositioning in the presence of the phenylalanyl-adenylate or its analogue is inevitable due to the interference. In our ternary complex, the CCA end does occupy a different position, adopting a hairpin conformation. The 3′ extremity of the tRNA approaches the active site in a way that A76 is placed in the vicinity of the AMP moiety of the PheOH-AMP analogue. The position of the 3′-terminal adenosine at the entrance to the active site cavity is held by formation of aromatic−aromatic interactions of two adenine rings and the histidine·adenine pair between the adenine base of the PheOH-AMP analogue and the imidazole ring of Hisα212, a PheRS-conserved motif 2 residue (Figure 5 and Table 2). Each interacting pair is characterized by an "edge-to-face" arrangement. Interestingly, the same type of interactions is employed for specific recognition of the phenylalanine (*26*). Moreover, Hisα212 may contribute to the positioning of Ade76 via a π−cation interaction between the protonated Nϵ2 atom of the imidazole ring and the aromatic portion of the terminal nucleotide. This type of interactions has been shown to be important for protein folding and implemented also as a driving force in protein−ligand recognition (*54*). Hydrogen bonding between the N7 atom of Ade76 and the guanidinium group of the motif 3-specific Argα321 contributes to further stabilization of the acceptor end.

Three loops are shown to be involved in closing up the active site of *T. thermophilus* PheRS. Two of them, namely, the class II-conserved motif 2 loop (residues 204−214 of the α subunit) and a helical loop (residues 139−152 of the α subunit), undergo conformational changes upon substrate binding (Figure 6). The helical loop stands for the mobile element [a PheRS-conserved xPxxHPAR(D/x)(M/x)(W/Q/H)DTF sequence] that contains a short helical ARD fragment and is functionally analogous to the structural elements of other class II aaRSs. The flipping loop of AspRS is one example of those (*11*). The motif 2 and helical loops move 1.6−1.8 Å toward the position of bound PheOH-AMP and the tRNA acceptor arm, as compared to the substrate-free structure. The displacement of the motif 2 loop is triggered by hydrogen bonding of a PheRS-conserved Gluα206 residue and the class II-invariant Argα204 with the 2′- and 3′-OH groups of the A76 ribose moiety (Table 2). An additional contact of the terminal 3′-OH group with the carbonyl oxygen of Metα148 from the helical loop (a conserved residue in bacteria) may have an appreciable effect on stabilization of this flexible region. As the helical loop changes its conformation, the position of Metα148 also changes (Figure 6). In the ternary complex, the side chain of this residue is displaced by ∼5 Å in comparison with the PheRS·Phe-AMP complex. The displacement of Metα148 prevents A76 from approaching the α-carbonyl carbon of PheOH-AMP. As a consequence, A76 occupies the position within the active site, which is unfavorable for the formation of the productive complex. The 2′-OH group of the ribose, the site of the primary amino acid attachment, is too distant from the α-carbonyl carbon of the amino acid moiety to react: the distance between these two atoms is ∼7 Å. It is notable that the helical loop adopts different conformations in the available PheRS structures, depending on the presence and nature of the ligand(s).

The third loop enveloping the active site is a PheRS-conserved x(Y/F)(F/N)P(F/Y)TEPS sequence (residues 256−264) of the α subunit. Two phenylalanines, Pheα258 and Pheα260, that play a key role in specific recognition of the amino acid substrate are invariant in all eubacterial PheRSs. We designate this PheRS-specific region as the FPF loop. In contrast to the two loops mentioned above, this loop shows a remarkably stable conformation of the backbone and the

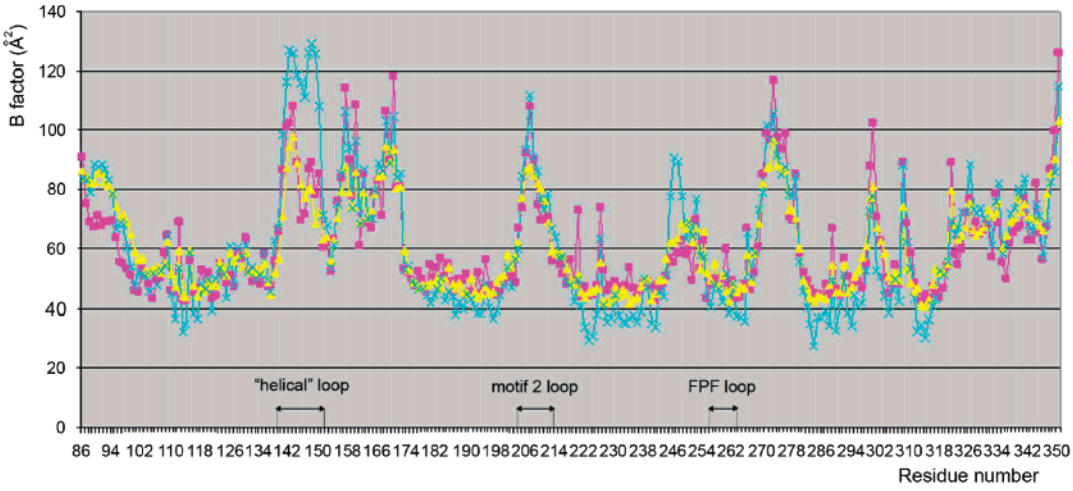

FIGURE 7: Relative mobility of different regions in the PheRS α subunit. Average temperature factors (in square angstroms) of the main chain atoms are shown for the native enzyme (purple) and its complexes with Phe-AMP (yellow) or PheOH-AMP (cyan). All *B* factors are given in a scale of the native PheRS. The helical loop (residues 139−152) is stabilized by interaction with the true intermediate in the PheRS·Phe-AMP complex but is significantly more flexible in the complex with the synthetic analogue.

amino acid side chains in all the complexes (as well as in the apoenzyme). The conformational stability is explained by the necessity to ensure the nearly rigid lock-and-key recognition mode of the phenylalanine.

Flexibility of the PheRS Structure Fragments. The temperature factors (*B* factors) are linearly related to the displacement of a particular atom or a group of atoms and, in general, characterize the conformational flexibility of structural fragments. On the basis of the coordinates of the complexes, the observed *B* factors were plotted versus the numbers of the α-subunit residues. The data of three structures, PheRS in the apo form and the complexes with Phe-AMP and PheOH-AMP, are presented in Figure 7. The graph demonstrates a high degree of flexibility of the helical loop (residues 139−152); among the three structures, the complex with PheOH-AMP exhibits the highest values of temperature factors. We emphasize that *B* factors of the complex with the native intermediate (Phe-AMP) have lower values when compared to that of the structure of the apoenzyme. In the ternary complex, the *B* factors associated with the helical loop fall into the range between those of the PheRS·Phe-AMP and PheRS·PheOH-AMP complexes.

DISCUSSION

The Conformational Changes Induced by the Small Substrates Exert Control *over the tRNA^{Phe} Binding Mode.* The structures of PheRS complexed with small substrates (Phe, Phe-AMP, or its stable analogue, PheOH-AMP) have exhibited structural changes within the catalytic domain, induced by these ligands (*25*, *26*). The binding of AMP or ATP promotes the displacement of the motif 2 loop. Binding of phenylalanine, free or bound to AMP, stabilizes the helical loop conformation. The binding of tRNA^{Phe} alone manifests only minor conformational changes in the active site area. It is formation of the phenylalanyl-adenylate in the course of the aminoacylation reaction that exerts the most pronounced effect on the active site rearrangement. The presence of the tRNA substrate and the phenylalanyl-adenylate analogue at one time enhances displacement of the loops toward the ligands. Concerted conformational changes ensure the correct order of substrate binding and reaction. It is apparent that cooperative structural dynamics is an important feature of the aminoacyl-tRNA synthetase activity.

The comparison of the tRNA^{Phe} binding modes in the binary PheRS·tRNA^{Phe} complex and our ternary complex has revealed a significant rearrangement of the CCA end. The conformational switch into the hairpin structure, induced by the analogue, stems from competition of Ade76 and the phenylalanine substrate for the binding site. Serα180, Gluα220, and Trpα149 as well as Pheα258 and Pheα260 were previously shown to interact with the phenylalanyl moiety of Phe-AMP and with Ade76 of tRNA^{Phe} in the respective binary PheRS complexes (*24*−*26*). Here, we have shown that the presence of the adenylate analogue enforces the 3′-terminal adenosine to adopt the new conformation that in turn allows the simultaneous positioning of all the reactants in the active site (Figure 5). The interactions of the enzyme with PheOH-AMP and tRNA^{Phe} induce concerted movements of the motif 2 and helical loops. Remarkably, that moderate displacement of the helical loop has a great deal to do with the organization of the active site and with significant conformational changes of Metα148 specifically. The side chain of Metα148 opens or closes a barrier for placing the tRNA^{Phe} CCA end within the active site, depending on whether the preassembled mode is productive or nonproductive. A clue about the "open" and "closed" conformation lies with interactions formed by Trpα149. In the complexes with a natively occurring phenylalanyl-adenylate or phenylalanine (*25*, *26*), Trpα149 participates in stabilization of the negatively charged carbonyl oxygen of the substrate, and the conformation of the helical loop may be specified as open, favorable for subsequent tRNA binding in the productive mode. The electron density for the side chain of Trpα149 is well-defined in the complex with Phe-AMP. The binding of the synthetic analogue (lacking the carbonyl oxygen) alone leads to destabilization of the helical loop, and it is evidenced by disorder of the electron density in the area of residues 148 and 149 (*25*). The reason is the absence of an intermolecular hydrogen bond between the ligand and Trpα149 and conformational changes induced by the van

der Waals repealing between the methylene group of PheOH-AMP and surrounding side chains. When $tRNA^{Phe}$ binds in the presence of the synthetic analogue, the helical loop appears to be clamped between the PheOH-AMP analogue and the CCA end. The induced-fit conformational changes trigger formation of a hydrogen bond between Metα148 and the O3′ atom of A76, thereby freezing the complex in the nonproductive mode. In the ternary complex, the electron density associated with the Trpα149 side chain reverts back to the ordered form. With regard to the structure, it corresponds to the closed conformation, in which the CCA end cannot be properly positioned to promote the second step of aminoacylation. Using a MD simulation, we further estimate the distance between the Nϵ1 atom of Trpα149 and the carbonyl oxygen of Phe-AMP at each instant of time; it fluctuates around a hydrogen bonding length. The availability of one intermolecular hydrogen bond stabilizes the helical loop within the catalytic domain framework; it is also evident from the ordering of the electron density. Conversely, the mobility of this fragment in the PheRS·PheOH-AMP complex is significantly increased (Figure 7) because of the lack of the carbonyl oxygen in the synthetic ligand. Thus, one can suggest that the capacity of the helical loop to open and close the active site is finely controlled by the nature of the substrate(s) bound.

The comparison of the binary PheRS·Phe-AMP and ternary PheRS·$tRNA^{Phe}$·PheOH-AMP complexes enables us to follow structural adjustment of the active site prior to the second step of the aminoacylation reaction. The conformational changes of the motif 2 loop upon Phe-AMP formation provide a framework for subsequent tRNA binding. The CCA end in the PheRS·$tRNA^{Phe}$ and PheRS·$tRNA^{Phe}$·PheOH-AMP complexes occupies two extreme positions preventing final charging of $tRNA^{Phe}$ from occurring. The orientation of A76 in the functional position most likely resembles that found in the ternary PheRS·$tRNA^{Phe}$·PheOH-AMP complex, and the CCA end possesses the hairpin conformation rather than the unwound one observed in the binary PheRS·$tRNA^{Phe}$ complex. The tRNA takes advantages of the fully extended conformation of Argα204 observed in the ternary complex: in addition to stabilization of Phe-AMP or PheOH-AMP, the guanidinium group of Argα204 forms a hydrogen bond with the sugar moiety of A76 (Figure 5). Gluα206 is the second residue of the motif 2 loop, which assists in the recognition of the adenine moiety of PheOH-AMP, both in the "tRNA-free" PheRS and in the ternary complex, and in the latter complex, it anchors additionally the tRNA 3′-terminal ribose. The class II-invariant Argα321 of motif 3 adopts an extended conformation during the first step of the aminoacylation reaction to stabilize the position of the newly synthesized phenylalanyl-adenylate. In the ternary complex, the conformation of Argα321 remains unchanged when interacting with the adenine ring of A76. The residue plays a universal role in ATP recognition through interactions with the adenine ring, the ribose moiety, and the γ-phosphate. The switch of Argα321 from the γ-phosphate to A76 recognition may thus trigger elimination of the pyrophosphate, terminating the stage of the amino acid activation.

The saturation of all hydrogen bonds in the enzyme−substrate complex occurs through the concerted move of the structural elements in the active site and induced-fit adjustment of the substrates to allow the phenylalanylation reaction. In this context, it is of interest to compare the frequency of hydrogen bond formation within the active site for Phe-AMP and PheOH-AMP ligands as it may be inferred from the 3D structures of the complexes. The dynamics of hydrogen bond formation in the vicinity of Phe-AMP and PheOH-AMP diverge considerably. An average number of hydrogen bonds formed by Phe-AMP or PheOH-AMP with surrounding side chains of the enzyme in the last 500 ps period is 3.6 or 1.3, respectively. This is a clear indication that the naturally occurring substrate forms more stable intermediates. As it also follows from the MD simulation, the stacking interaction between Pheα216 and the adenylate ring demonstrates the highest stability among the all possible types of interactions in the environment where Phe-AMP is embedded: the stacking conformation remains unchanged during the period of 1 ns.

Movements of various loops and side chains create a buried pocket perfectly designed for the peculiar phenylalanylation reaction governed by stepwise adjustment of all the reactants and intermediates in the active site. In the first step, phenylalanine binds in the amino acid-binding pocket in the orientation favorable for binding of ATP. Both substrates are located at the active site of PheRS in accordance with an in-line mechanism for the phenylalanine activation to occur. At this stage, water molecule S620 (PDB entry 1PYS), previously found to stabilize the helical loop in the native structure, is forced out from the active site. The first step of aminoacylation is essential for stabilization of the helical loop in its open conformation via the hydrogen bonding between the carbonyl oxygen of the intermediate and Trpα149. As this takes place, the side chain of Metα148 is held in the open conformation corresponding to that described in the complex with Phe-AMP. To accomplish the transfer of the amino acid moiety to the 2′-OH group of $tRNA^{Phe}$, the latter must be positioned ~3.5 Å from the α-carbonyl carbon of the phenylalanyl-adenylate. The attempts to bring the 3′-OH group (the characteristic site of primary amino acid attachment by class II aaRSs) of the 3′-terminal ribose into a favorable position for a nucleophilic attack on the first intermediate product lead to significant rearrangement of the active site topology. When all the reactants at this stage are properly positioned, there is no sterical hindrance for location of the CCA end at the active site in the conformation suitable for the second step of the phenylalanylation reaction to proceed. Thus, we may conclude that the aminoacylation stereochemistry of class I is the idiosyncratic feature of the PheRS system, which structurally belongs to class II aaRSs.

Comparison of the Crystal Structure and Solution Studies. The interactions of *T. thermophilus* PheRS with the $tRNA^{Phe}$ acceptor end have been explored in solution studies. The 3′ end binding in the absence or presence of phenylalanine and ATP was analyzed by an affinity cross-linking technique, using $tRNA^{Phe}$ derivatives substituted with 4-thiouridine (s^4U) at the 3′ end or specifically oxidized with periodate (*32*, *33*). The effects produced by binding of ATP on the total cross-linking efficiency and distribution of cross-links to the α and β subunits far exceed those of phenylalanine; in the presence of the two substrates, they are largely similar to those of ATP. These results agree with a primary role assigned to ATP or AMP in positioning of the acceptor end,

as revealed by the ternary complex structure: the adenine base of PheOH-AMP is directly involved in binding of A76; most residues interacting with AMP or ATP contribute also to the A76 recognition. The competition of A76 with AMP or ATP for the interactions with the catalytic site residues can explain the noticeable protective effect of ATP on the α-subunit cross-linking (a 2.2−2.4-fold decrease in the efficiency as compared to that in the absence of ATP), observed in the experiments with two different reactive probes. Similar patterns of the phenylalanine- and ATP-induced effects on the interaction with the $tRNA^{Phe}$ 3′ end have been found in the cross-linking study of human cytoplasmic PheRS (*34*), thus suggesting conservation of the molecular mechanism ensuring the precise positioning of the acceptor end in the catalytic site of tetrameric PheRSs. Indeed, most of the residues cooperating in binding and recognition of the AMP moiety and A76 are class II-invariant or strictly conserved in all PheRSs (Table 2). At the same time, two key residues of the helical loop, Metα148 and Trpα149, whose interactions with substrates additionally control the productive binding of the tRNA terminal ribose, are not conserved. The biochemical and structural data combined with phylogenetic analyses suggest that the general mechanism of tRNA phenylalanylation involves both conserved and species-specific interactions.

The functional role of the universal CCA end in the $tRNA^{Phe}$−PheRS interaction was examined by steady-state aminoacylation of 3′-end-modified tRNAs (*32*, *34*, *55*). $tRNA^{Phe}$ variants terminating in cytidine or 6-thioguanosine (s^6G) are substrates for aminoacylation by *T. thermophilus* PheRS, having a catalytic efficiency (k_{cat}/K_m) significantly lower (140- or 370-fold, respectively) than that of wild-type $tRNA^{Phe}$, mostly due to a decrease in k_{cat}. Uridine or its close homologue s^4U cannot substitute for A76 in the $tRNA^{Phe}$ aminoacylation by three PheRSs that were tested (from *T. thermophilus*, *E. coli*, and humans). The positive effect of the purine ring on aminoacylation is evident from the structure presented here. It is the interaction of the N7 atom with Argα321 that contributes to the A76 recognition and, furthermore, may control dissociation of the pyrophosphate, thus further affecting the turnover rate of the reaction. The exocyclic 6-amino group whose importance was suggested from the kinetic measurements is not specifically recognized in the ternary complex. The observed selectivity in aminoacylation of the 3′-end-modified tRNAs (A > C > s^6G > U and s^4U) may reflect various mixed capacities of the replacing nucleobases to form the base-specific, aromatic, and π−cation interactions necessary for the proper positioning in the active site. The penultimate cytidines at the CCA end are also essential for the $tRNA^{Phe}$ aminoacylation. *T. thermophilus* and *E. coli* $tRNA^{Phe}$ variants terminating in the UUA group were shown to be charged by the homologous PheRSs with efficiencies 8-fold lower compared to those of the wild-type substrates. The reduced activity may be explained by the loss of the base-specific contacts (of C75), shown in our structure to stabilize the acceptor end conformation. A nonconservative replacement of both cytidines with A yielded quite poor if any substrates for the bacterial enzymes, which may be due to primary changes in the structure and/or stability of the 3′ end, modulating in turn its binding. The mutational effects of the CCA end, contributing mostly to the interaction of the acceptor arm with PheRS, are significantly stronger than those of the discriminator base: the decrease in the k_{cat}/K_m of $tRNA^{Phe}$ aminoacylation by *T. thermophilus* PheRS observed only when A73 was replaced with a pyrimidine (U or C) does not exceed 2-fold (*47*). This result is consistent with an indirect role of A73 in the $tRNA^{Phe}$ recognition: this nucleotide further stabilizes the hairpin conformation of the acceptor end via its intra-RNA interactions.

The structural analysis shows six nucleotides (16, 17, 20, 33, 44, and 47) from three loops of $tRNA^{Phe}$ represent major points of long-range rearrangement of the substrate in complex with PheRS: they change conformation, depending on the presence of the PheOH-AMP analogue. The functional implication of most of these nucleotides in the complex adjustment through an induced fit is evidenced by independent biochemical data obtained previously for *T. thermophilus* PheRS. Nucleotides 20, 33, 45 (adjacent to nucleotide 44), and 47 were shown to form s^4U-induced cross-links with PheRS subunits (*31*), indicating that contacts not observed in the crystal structures are transiently formed upon the PheRS−$tRNA^{Phe}$ interaction. Nucleotides 16 and 44 are among those whose cleavage by iodine in the phosphorothioate footprinting experiments was shown to be enhanced (*30*). This result supports the idea of deformation of the respective $tRNA^{Phe}$ regions upon binding with PheRS. The conformational flexibility of nucleotides 16 and 17 is evident from the high-resolution structures of yeast $tRNA^{Phe}$ (*48*, *49*). Moreover, the position of D16 in free yeast $tRNA^{Phe}$ is shown to be sensitive to ionic conditions: it pairs with U59 when Mn^{2+} or Co^{2+} is present in the crystals but points away from U59 in the presence of Mg^{2+} (*48*). U20 and G44 contribute to $tRNA^{Phe}$ recognition at the level of binding and catalysis, and the specificity of U16 is only slightly displayed at the binding step (*29*, *47*); U33 and U47 were not tested for potential recognition by PheRSs (*28*). A comparison of binding and aminoacylation properties of $tRNA^{Phe}$ variants revealed that effects of mutations at the A26·G44 base pair and position 20 are quite different from those of the other variants (*29*): the most pronounced reduction in the turnover rates of aminoacylation (k_{cat}) corresponds to the smallest increase in the dissociation constants. The observed correlation is consistent with the idea that the increased stability of the complex makes it unable to adopt the correct conformation required at the transition state of the aminoacylation reaction. Notably, the G19·C56 tertiary base pair and U45·G10·C25 base triple, proposed to contribute primarily to stabilization of the correctly folded $tRNA^{Phe}$ structure (*29*), exhibit stable conformations in the two complexes: PheRS·$tRNA^{Phe}$ and PheRS·$tRNA^{Phe}$·PheOH-AMP. The structural and biochemical data combined indicate that U16, U20, and the A26·G44 base pair contribute indirectly to the $tRNA^{Phe}$ recognition via adjustment of the tRNA structure upon its interaction with the enzyme. Further evidence of the PheOH-AMP-induced rearrangement of the PheRS·$tRNA^{Phe}$ complex, which extends from the acceptor end to the anticodon loop, comes from study of the formation of the complex between yeast PheRS and cognate tRNA detected by Y37 base fluorescence (*56*).

Class- and System-Specific Characteristics of PheRS Control Binding of the $tRNA^{Phe}$ Acceptor End. Residues and regions of PheRS responsible for the proper positioning of the tRNA 3′ CCA end toward the active site are now

identified, thus enabling analysis of their class-conserved or system-specific role in the aminoacylation reaction. The two flexible regions, the motif 2 and helical loops, which form a network of interactions with the terminal nucleotide, A76, are common features of class II aaRSs. The motif 2 loop plays a universal role, cooperating in binding of ATP and of the acceptor arm in all known structures of class II aaRSs. The involvement of the class II-invariant arginine of this loop in binding of A76 is a common characteristic of ThrRS (*15*) and PheRS, representatives of subclasses IIa and IIc, respectively; in PheRS, the interaction of the motif 2 loop with A76 is reinforced by contacts of two system-conserved residues, Gluα206 and Hisα212, with the ribose and adenine moieties, respectively. The helical loop is topologically equivalent to the so-called ordering loop in subclass IIa enzymes, ThrRS, ProRS, and HisRS (*15*), and to the flipping loop in subclass IIb AspRS (*10*, *11*). The ordering loop in ThrRS plays an essential role in the second step of the aminoacylation reaction, contributing mainly to stabilization of A76; it closes the active site cavity when three substrates are bound. A conformational switch of the flipping loop of AspRS from the adenylate (a closed conformation) to the tRNA-binding position (an open conformation) controls the two steps of the aspartylation reaction. The helical loop in PheRS is exercising control over the aminoacyl-adenylate and tRNA substrate binding; its open conformation stabilized by interaction with the intermediate favors the proper positioning of A76. The class-conserved motif 3 arginine, contributing universally to ATP recognition, is involved in the CCA end binding in two systems: in our PheRS structure, it completes the network of interactions with A76, forming a hydrogen bond with the base; in *E. coli* AspRS, it anchors the base of C75 (*11*). The conformational switch of this residue from the γ-phosphate of ATP to tRNA binding may favor completion of the first step of the aminoacylation reaction. A similar role in the ThrRS system is performed by a second class-conserved motif 2 arginine stabilizing the position of C74 (*15*). Additional flexible regions of ThrRS and AspRS shown to contribute to the proper positioning of the CCA end all belong to the catalytic domain (*10*, *11*, *15*). In ThrRS, these are Thr- and ATP-binding loops, whose conformations depend mainly on the presence of the amino acid and ATP, respectively. In AspRSs, these are system-conserved amino acid-binding fragments: Q(S/A)PQ motif [topologically equivalent to the class-conserved TxE loop absent only in ThrRS (*57*)] and a eubacterial- and eukaryotic-specific loop. The involvement of two noncatalytic domains (B1 and B3) in positioning of the CCA end is dictated by a strictly specified trajectory by which PheRS may approach $tRNA^{Phe}$, when the anticodon arm has been clamped between the coiled-coil and B8 domains of the enzyme. In other words, it is a consequence of the PheRS structural organization wherein one $tRNA^{Phe}$ molecule binds across all four subunits and is properly a unique feature of the phenylalanine-specific system.

ACKNOWLEDGMENT

We thank Valentina Ankilova for expert assistance with enzyme preparation, Yehuda Goldgur for help in data collection and for fruitful discussions, and Olga Lavrik for interest in the work.

REFERENCES

1. Eriani, G., Delarue, M., Poch, O., Gangloff, J., and Moras, D. (1990) Partition of tRNA synthetases into two classes based on mutually exclusive sets of sequence motifs, *Nature 347*, 203−206.
2. Cusack, S., Berthet-Colominas, C., Härtlein, M., Nassar, N., and Leberman, R. (1990) A second class of synthetase structure revealed by X-ray analysis of *E. coli* seryl-tRNA synthetase at 2.5 Å resolution, *Nature 347*, 249−255.
3. Fraser, T. H., and Rich, A. (1975) Amino acids are not all initially attached to the same position on transfer RNA molecules, *Proc. Natl. Acad. Sci. U.S.A. 72*, 3044−3048.
4. Sprinzl, M., and Cramer, F. (1975) Site of aminoacylation of tRNAs from *E. coli* with respect to the 2′- or 3′-hydroxyl group of the terminal adenosine, *Proc. Natl. Acad. Sci. U.S.A. 72*, 3049−3053.
5. First, E. A. (2005) Catalysis of the tRNA aminoacylation reaction, in *The Aminoacyl-tRNA Synthetases* (Ibba, M., Francklyn, C., and Cusack, S., Eds.) pp 328−347, Landes Bioscience, Georgetown, TX.
6. Arnez, J. G., and Moras, D. (1997) Structural and functional considerations of the aminoacylation reaction, *Trends Biochem. Sci. 22*, 211−216.
7. Cusack, S. (1997) Aminoacyl-tRNA synthetases, *Curr. Opin. Struct. Biol. 7*, 881−889.
8. Giegé, R., Sissler, M., and Florentz, C. (1998) Universal rules and idiosyncratic features in tRNA identity, *Nucleic Acids Res. 26*, 5017−5035.
9. Cavarelli, J., Eriani, G., Rees, B., Ruff, M., Boeglin, M., Mitschler, A., Martin, F., Gangloff, J., Thierry, J.-C., and Moras, D. (1994) The active site of yeast aspartyl-tRNA synthetase: Structural and functional aspects of the aminoacylation reaction, *EMBO J. 15*, 327−337.
10. Sauter, C., Lorber, B., Cavarelli, J., Moras, D., and Giegé, R. (2000) The free yeast aspartyl-tRNA synthetase differs from the $tRNA^{Asp}$-complexed enzyme by structural changes in the catalytic site, hinge region, and anticodon-binding domain, *J. Mol. Biol. 299*, 1313−1324.
11. Eiler, S., Dock-Bregeon, A.-C., Moulinier, L., Thierry, J.-C., and Moras, D. (1999) Synthesis of aspartyl-$tRNA^{Asp}$ in *Escherichia coli*: A snapshot of the second step, *EMBO J. 18*, 6532−6541.
12. Rees, B., Webster, G., Delarue, M., Boeglin, M., and Moras, D. (2000) Aspartyl-tRNA synthetase from *Escherichia coli*: Flexibility and adaptability to the substrates, *Mol. Biol. 23*, 1157−1164.
13. Briand, C., Poterszman, A., Eiler, S., Webster, G., Thierry, J.-C., and Moras, D. (2000) An intermediate step in the recognition of $tRNA^{Asp}$ by aspartyl-tRNA synthetase, *J. Mol. Biol. 299*, 1051−1060.
14. Cusack, S., Yaremchuk, A., and Tukalo, M. (1996) The crystal structure of the ternary complex *of T. thermophilus* seryl-tRNA synthetase with $tRNA^{Ser}$ and a seryl-adenylate analogue reveals a conformational switch in the active site, *EMBO J. 15*, 2834−2842.
15. Torres-Larios, A., Sankaranarayanan, R., Rees, B., Dock-Bregeon, A.-C., and Moras, D. (2003) Conformational movements and cooperativity upon amino acid, ATP and tRNA binding in threonyl-tRNA synthetase, *J. Mol. Biol. 331*, 201−211.
16. Yaremchuk, A., Tukalo, M., Grøtli, M., and Cusack, S. (2001) A succession of substrate induced conformational changes ensures the amino acid specificity of *Thermus thermophilus* prolyl-tRNA synthetase: Comparison with histidyl-tRNA synthetase, *J. Mol. Biol. 309*, 989−1002.
17. Cusack, S., Yaremchuk, A., and Tukalo, M. (1996) The crystal structures of *T. thermophilus* lysyl-tRNA synthetase complexed with *E. coli* $tRNA^{Lys}$ and a *T. thermophilus* $tRNA^{Lys}$ transcript: Anticodon recognition and conformational changes upon binding of a lysyl-adenylate analogue, *EMBO J. 15*, 6321−6334.
18. Desogus, G., Todone, F., Brick, P., and Onesti, S. (2000) Active site of lysyl-tRNA synthetase: Structural studies of the adenylation reaction, *Biochemistry 39*, 8418−8425.
19. Berthet-Colominas, C., Seignovert, L., Hartlein, M., Grøtli, M., Cusack, S., and Leberman, R. (1998) The crystal structure of asparaginyl-tRNA synthetase from *Thermus thermophilus* and its complexes with ATP and asparaginyl-adenylate: The mechanism of discrimination between asparagine and aspartic acid, *EMBO J. 17*, 2947−2960.

20. Rath, V. L., Silvian, L. F., Beijer, B., Sproat, B. S., and Steitz, T. A. (1998) How glutaminyl-tRNA synthetase selects glutamine, *Structure 6*, 439−449.
21. Delagoutte, B., Moras, D., and Cavarelli, J. (2000) tRNA aminoacylation by arginyl-tRNA-synthetase: Induced conformations during substrates binding, *EMBO J. 19*, 5599−5610.
22. Sekine, S., Nureki, O., Dubois, D. Y., Bernier, S., Chênevert, R., Lapointe, J., Vassylyev, D. G., and Yokoyama, S. (2003) ATP binding by glutamyl-tRNA synthetase is switched to the productive mode by tRNA binding, *EMBO J. 22*, 676−688.
23. Mosyak, L., Reshetnikova, L., Goldgur, Y., Delarue, M., and Safro, M. (1995) Structure of phenylalanyl-tRNA synthetase from *Thermus thermophilus*, *Nat. Struct. Biol. 2*, 537−547.
24. Goldgur, Y., Mosyak, L., Reshetnikova, L., Ankilova, V., Khodyreva, S., Lavrik, O., and Safro, M. (1997) The crystal structure of phenylalanyl-tRNA synthetase from *Thermus thermophilus* complexed with cognate $tRNA^{Phe}$, *Structure 5*, 59−68.
25. Reshetnikova, L., Moor, N., Lavrik, O., and Vassylyev, D. (1999) Crystal structures of phenylalanyl-tRNA synthetase complexed with phenylalanine and a phenylalanyl-adenylate analogue, *J. Mol. Biol. 287*, 555−568.
26. Fishman, R., Ankilova, V., Moor, N., and Safro, M. (2001) Structure at 2.6 Å resolution of phenylalanyl-tRNA synthetase complexed with phenylalanyl-adenylate in the presence of manganese, *Acta Crystallogr. D57*, 1534−1544.
27. Kotik-Kogan, O., Moor, N., Tworowski, D., and Safro, M. (2005) Structural basis for discrimination of L-phenylalanine from L-tyrosine by phenylalanyl-tRNA synthetase, *Structure 13*, 1799−1807.
28. Safro, M., Moor, N., and Lavrik, O. (2004) Phenylalanyl-tRNA synthetase, in *The Aminoacyl-tRNA synthetases* (Ibba, M., Francklyn, C., and Cusack, S., Eds.) pp 250−265, Landes Bioscience, Georgetown, TX.
29. Vasil'eva, I., Ankilova, V., Lavrik, O., and Moor, N. (2002) tRNA discrimination by *T. thermophilus* phenylalanyl-tRNA synthetase at the binding step, *J. Mol. Recognit. 15*, 188−196.
30. Kreutzer, R., Kern, D., Giegé, R., and Rudinger, J. (1995) Footprinting of $tRNA^{Phe}$ transcripts from *Thermus thermophilus* HB8 with homologous phenylalanyl-tRNA synthetase reveals a novel mode of interaction, *Nucleic Acids Res. 23*, 4598−4602.
31. Moor, N. A., Ankilova, V. N., Lavrik, O. I., and Favre, A. (2001) Determination of $tRNA^{Phe}$ nucleotides contacting the subunits of *Thermus thermophilus* phenylalanyl-tRNA synthetase by affinity crosslinking, *Biochim. Biophys. Acta 1518*, 226−236.
32. Vasil'eva, I. A., Ankilova, V. N., Lavrik, O. I., and Moor, N. A. (2000) Interaction of *T. thermophilus* phenylalanyl-tRNA synthetase with the 3′-terminal nucleotide of $tRNA^{Phe}$, *Biochemistry (Moscow) 65*, 1157−1166.
33. Vasil'eva, I. A., Bogachev, V. S., Favre, A., Lavrik, O. I., and Moor, N. A. (2004) Role of low-molecular-weight substrates in functional binding of the $tRNA^{Phe}$ acceptor end by phenylalanyl-tRNA synthetase, *Biochemistry (Moscow) 69*, 179−191.
34. Moor, N., Lavrik, O., Favre, A., and Safro, M. (2003) Prokaryotic and eukaryotic tetrameric phenylalanyl-tRNA synthetases display conservation of the binding mode of the $tRNA^{Phe}$ CCA end, *Biochemistry 42*, 10697−10708.
35. Ankilova, V., Reshetnikova, L., Chernaya, M., and Lavrik, O. (1988) Phenylalanyl-tRNA synthetase from *Thermus thermophilus* HB8. Purification and properties of the crystallizing enzyme, *FEBS Lett. 227*, 9−13.
36. Watanabe, K., Oshima, T., Iijima, K., Yamaizumi, Z., and Nishimura, S. (1980) Purification and thermal stability of several amino acid-specific tRNAs from an extreme thermophile, *Thermus thermophilus* HB8, *J. Biochem. 87*, 1−13.
37. Bischoff, R., and McLaughlin, L. W. (1985) Isolation of specific tRNAs using an ionic-hydrophobic mixed-mode chromatographic matrix, *Anal. Biochem. 151*, 526−533.
38. Lavrik, O., Moor, N., and Nevinskii, G. (1978) Synthesis of analogs of L-phenylalanyladenylate and study of their interactions with *E. coli* phenylalanyl-tRNA synthetase, *Bioorg. Khim. 4*, 1470−1487.
39. Reshetnikova, L., Khodyreva, S., Lavrik, O., Ankilova, V., Frolow, F., and Safro, M. (1993) Crystals of the phenylalanyl-tRNA synthetase from *Thermus thermophilus* HB8 complexed with $tRNA^{Phe}$, *J. Mol. Biol. 231*, 927−929.
40. Otwinowski, Z., and Minor, W. (1996) Processing of X-ray diffraction data collected processing in oscillation mode, *Methods Enzymol. 276*, 307−326.
41. Brunger, A., Adams, P., Clore, G., DeLano, W., Gros, P., Grosse-Kunstleve, R., Jiang, J., Kuszewski, J., Nigles, M., Pannu, N., Read, R., Rice, L., Simonson, T., and Warren, G. (1998) Crystallography & NMR system: A new software suite for macromolecular structure determination, *Acta Crystallogr. D54*, 905−921.
42. Jones, T., Zou, J., Cowtan, S., and Kjeldgaard, M. (1991) Improved methods for building protein models in electron density maps and the location of errors in these models, *Acta Crystallogr. A47*, 110−119.
43. Berendsen, H., van der Spoel, D., and van Drunen, R. (1995) GROMACS: A message-passing parallel molecular dynamic implementation, *Comput. Phys. Commun. 91*, 43−56.
44. Lindahl, E., Hess, B., and van der Spoel, D. (2001) GROMACS 3.0: A package for molecular simulation and trajectory analysis, *J. Mol. Model. 7*, 306−317.
45. van Gunsteren, W., Billeter, S., Eising, A., Hunenberger, P., Kruger, P., Mark, A., Scott, W., and Tironi, I. (1996) *Biomolecular Simulation*: *The GROMOS96 Manual and User Guide*, Hochshulverlag AG an der ETH, Zurich, Switzerland.
46. Schüttelkopf, A. W., and van Aalten, D. M. F. (2004) PRODRG: A tool for high-throughput crystallography of protein-ligand complexes, *Acta Crystallogr. D60*, 1355−1363.
47. Moor, N. A., Ankilova, V. N., and Lavrik, O. I. (1995) Recognition of $tRNA^{Phe}$ by phenylalanyl-tRNA synthetase of *Thermus thermophilus*, *Eur. J. Biochem. 234*, 897−902.
48. Shi, H., and Moore, P. B. (2000) The crystal structure of yeast phenylalanine tRNA at 1.93 Å resolution: A classic structure revisited, *RNA 6*, 1091−1105.
49. Jovine, L., Djordjevic, S., and Rhodes, D. (2000) The crystal structure of yeast phenylalanine tRNA at 2.0 Å resolution: Cleavage by Mg^{2+} in 15-year old crystals. *J. Mol. Biol. 301*, 401−414.
50. Durant, P. C., and Davis, D. R. (1999) Stabilization of the anticodon stem-loop of $tRNA^{Lys,\ 3}$ by an A^{+}-C base-pair and by pseudouridine, *J. Mol. Biol. 285*, 115−131.
51. Rees, B., and Moras, D. (1996) Conformational flexibility of tRNA: Structural changes in yeast $tRNA^{Asp}$ upon binding to aspartyl-tRNA synthetase, *Biochimie 78*, 624−631.
52. Cusack, S., Yaremchuk, A., Krikliviy, I., and Tukalo, M. (2001) $tRNA^{Pro}$ anticodon recognition by *Thermus thermophilus* prolyl-tRNA synthetase, *Structure 6*, 101−108.
53. Auffinger, P., and Westhof, E. (2001) An extended structural signature for the tRNA anticodon loop, *RNA 7*, 334−341.
54. Ma, J. C., and Dougherty, D. A. (1997) The cation-π interaction, *Chem. Rev. 97*, 1303−1324.
55. Moor, N. A., Repkova, M. N., Yamkovoy, V. I., and Lavrik, O. I. (1994) Alterations at the 3′-CCA end of *Escherichia coli* and *Thermus thermophilus* $tRNA^{Phe}$ do not abolish their acceptor activity, *FEBS Lett. 351*, 241−242.
56. Krauss, G., von der Haar, F., and Maass, G. (1979) Conformational transitions of a tRNA-aminoacyl-tRNA synthetase complex induced by tRNAs bearing different modifications in the 3′ terminus, *Biochemistry 18*, 4755−4761.
57. Belrhali, H., Yaremchuk, A., Tukalo, M., Larsen, K., Berthet-Colominas, C., Leberman, R., Beijer, B., Sproat, B., Als-Nielsen, J., Grübel, G., Legrand, J. F., Lehmann, M., and Cusack, S. (1994) Crystal structures at 2.5 angstrom resolution of seryl-tRNA synthetase complexed with two analogs of seryl adenylate, *Science 263*, 1432−1436.

BI060491L